Geophysical Research Letters®

Dissimilar Sensitivities of Ocean Acidification Metrics to Anthropogenic Carbon Accumulation in the Central North Pacific Ocean and California Current Large Marine Ecosystem

Mar C. Arroyo[1] , Andrea J. Fassbender[2,3] , Brendan R. Carter[2,4] , Christopher A. Edwards[1] , Jerome Fiechter[1] , Addie Norgaard[3,5] , and Richard A. Feely[2]

[1]Department of Ocean Sciences, University of California Santa Cruz, Santa Cruz, CA, USA, [2]NOAA/OAR Pacific Marine Environmental Laboratory, Seattle, WA, USA, [3]Monterey Bay Aquarium Research Institute, Moss Landing, CA, USA, [4]Cooperative Institute for Climate, Ocean, and Ecosystem Studies, University of Washington, Seattle, WA, USA, [5]University of Alaska Fairbanks, Fairbanks, AK, USA

Abstract We analyze and compare changes in ocean acidification metrics caused by anthropogenic carbon ($\mathrm{C_{anth}}$) accumulation in the North Pacific Ocean and California Current Large Marine Ecosystem (CCLME). The greatest declines in pH and carbonate mineral saturation state occur near the surface, coincident with the highest $\mathrm{C_{anth}}$ concentrations. However, maximal increases in the partial pressure of carbon dioxide ($p\mathrm{CO}_2$) and hydrogen ion concentration occur subsurface where $\mathrm{C_{anth}}$ values are lower. We attribute dissimilar sensitivities of these metrics to background ocean chemistry, which has naturally high $p\mathrm{CO}_2$ and low buffering capacity in subsurface waters due to accumulated byproducts of organic matter respiration, which interacts with $\mathrm{C_{anth}}$. In the CCLME, rising subsurface $p\mathrm{CO}_2$ has increased the frequency, duration, and intensity of hypercapnia ($p\mathrm{CO}_2 \geq 1{,}000$ μatm) on the continental shelf. Our findings suggest that hypercapnia induced by $\mathrm{C_{anth}}$ accumulation can co-occur with hypoxia in the CCLME and is an additional modern stressor for marine organisms.

Plain Language Summary The ocean mitigates the extent of global warming by absorbing a portion of the carbon dioxide gas (CO_2) released into the atmosphere by human activities. However, this comes at a cost to ocean health because the uptake of this anthropogenic CO_2 causes changes in ocean chemistry, called ocean acidification (OA), that can be detrimental to marine ecosystems. This study explores how OA metrics have changed in the upper waters of the open North Pacific Ocean and coastal California Current Large Marine Ecosystem (CCLME). We focus on the CCLME due to its global importance and economically important fisheries. We find that different OA metrics exhibit different patterns of change with depth in the water column due to the natural, background ocean chemistry. One such metric shows that there is now more subsurface water containing CO_2 levels elevated enough to threaten the health of marine organisms than there was before the anthropogenic CO_2 addition. Our finding of expanded volumes of water with high-CO_2 levels near the coast is important to consider as a source of stress for marine organisms living both on the seafloor and in the water column.

1. Introduction

The ocean has absorbed ∼25% of the carbon dioxide released to the atmosphere by anthropogenic activities since the preindustrial (PI) era, leading to measurable changes in ocean chemistry (Friedlingstein et al., 2022). Increases in surface ocean carbon dioxide partial pressure ($p\mathrm{CO}_2$) cause associated increases in hydrogen ion concentration ($[\mathrm{H}^+]$) and declines in pH ($-\log_{10}([\mathrm{H}^+])$) and carbonate ion concentration ($[\mathrm{CO}_3^{2-}]$; Caldeira & Wickett, 2003; Feely et al., 2004, 2008). Such chemical changes due to anthropogenic carbon ($\mathrm{C_{anth}}$) accumulation are collectively referred to as ocean acidification (OA) and have widespread implications for the health of marine organisms and ecosystems (Doney et al., 2020; Gattuso et al., 2015; Orr et al., 2005).

Two common metrics used to assess the progression and potential impact of OA on marine organisms are pH and the saturation state of calcium carbonate minerals, such as aragonite (Ω_{Ar}). Numerous prior works have shown that these metrics, and others, vary distinctly in their response to rising surface ocean $p\mathrm{CO}_2$ (Bates et al., 2014; Cai

et al., 2020; Feely et al., 2004, 2009; Jiang et al., 2019; Lauvset et al., 2015), due in part to differing sensitivities of each parameter to environmental conditions (Bittig et al., 2018; Egleston et al., 2010; Fassbender et al., 2017; Hagens & Middelburg, 2016; Riebesell et al., 2009). Fewer studies have considered how OA metrics evolve below the air-sea interface in response to carbon accumulation (Cai et al., 2011; Carter et al., 2019; Fassbender et al., 2021; Feely et al., 2018; Jiang et al., 2015; Lauvset et al., 2020; Resplandy et al., 2013; Ríos et al., 2015), and the findings suggest dissimilar carbonate system property perturbations with depth.

A less-emphasized OA metric of growing concern is the volume of water with in situ pCO_2 exceeding 1,000 µatm (hypercapnia; McNeil & Sasse, 2016). Hypercapnia has been shown to negatively interfere with physiological and neurological functions in fishes and other marine organism by hindering organismal ability to excrete CO_2 during respiration and by disrupting internal acid-base regulation (Nilsson et al., 2012; Perry & Gilmour, 2006). Hypercapnic conditions can already be found in modern ocean environments, including upwelling regions like the California Current Large Marine Ecosystem (CCLME) in the Northeast Pacific Ocean (Feely et al., 2018). In this region, seasonal, wind-driven upwelling along the US West Coast transports subsurface waters, naturally low in pH, Ω_{Ar}, and dissolved oxygen (O_2) and elevated in pCO_2 due to prior organic matter remineralization, to the continental shelf environment (Feely et al., 2008; Gruber et al., 2012; Hauri et al., 2009, 2013). Subsurface remineralization inherently links high pCO_2 and low pH values to low O_2 values, which can be intensified on the continental shelf by locally driven processes (Chan et al., 2017, 2019; Feely et al., 2016, 2018). During the upwelling season, certain coastal regions in the CCLME can experience severe hypoxic conditions ($[O_2] \leq 60$ µmol kg^{-1}; Connolly et al., 2010; Grantham et al., 2004; Peterson et al., 2013). The potential expansion and intensification of hypercapnic zones in the CCLME with continued C_{anth} accumulation poses a risk to organisms already exposed to spatially nonuniform stressors of acidification and hypoxia (Cheresh & Fiechter, 2020; Feely et al., 2018; McNeil & Sasse, 2016), in combination with ocean warming (Kroeker et al., 2013).

In this study, we evaluate and compare changes in OA metrics caused by C_{anth} accumulation in the Central North Pacific Ocean (CNPO) and the CCLME since industrialization. Our study builds on the prior efforts of Feely et al (2016) and Carter et al. (2019) to extend North Pacific Ocean C_{anth} estimates to the US West Coast. We focus on the vertical structure of C_{anth}-sensitivity for pH, Ω_{Ar}, pCO_2, and [H$^+$] and consider the impact of subsurface changes on the habitable zones of marine organisms in the CCLME. We then use output from a regional ocean model to examine the frequency, intensity, and duration at which the modern-day shelf ecosystem experiences conditions of hypercapnia.

2. Methods

2.1. Cruise Data and Derived Carbonate System Parameters

We use observational data from the 2015 CLIVAR/GO-SHIP P16 N Leg 2 cruise (Cross et al., 2017) in the CNPO and from the 2016 West Coast Ocean Acidification (WCOA2016) cruise (Alin et al., 2017; Figure 1) in the CCLME. Discrete measurements of the dissolved inorganic carbon (DIC), total alkalinity (TA), O_2, and inorganic nutrients (phosphate and silicate) were collected from each station, in addition to vertical conductivity-temperature-depth profiles. P16 N stations between 22.5°N and 56°N and WCOA transects between 25°N and 54°N are used herein. DIC and TA concentrations were measured on board each cruise by coulometric titration (Johnson et al., 1993) and open-cell potentiometric titration (Millero et al., 1993), respectively, following standard procedures (Dickson et al., 2007). Routine analysis of Certified Reference Materials (Dickson et al., 2003) and replicate samples ensured DIC and TA uncertainties were better than ±0.1%. O_2 concentration was determined by a modified Winkler titration (Carpenter, 1965) with an uncertainty of ±1.4 µmol kg^{-1}.

Additional carbonate system parameters were calculated from DIC, TA, temperature, salinity, phosphate, and silicate using CO2SYSv1.1 for MATLAB (Lewis & Wallace, 1998; van Heuven et al., 2011) with the dissociation constants for carbonic acid by Lueker et al. (2000), bisulfate ion by Dickson (1990), and total boron by Uppström (1974). Calculated parameters include in situ pH on the total scale, Ω_{Ar}, pCO_2, [H$^+$], and Revelle Factor (RF).
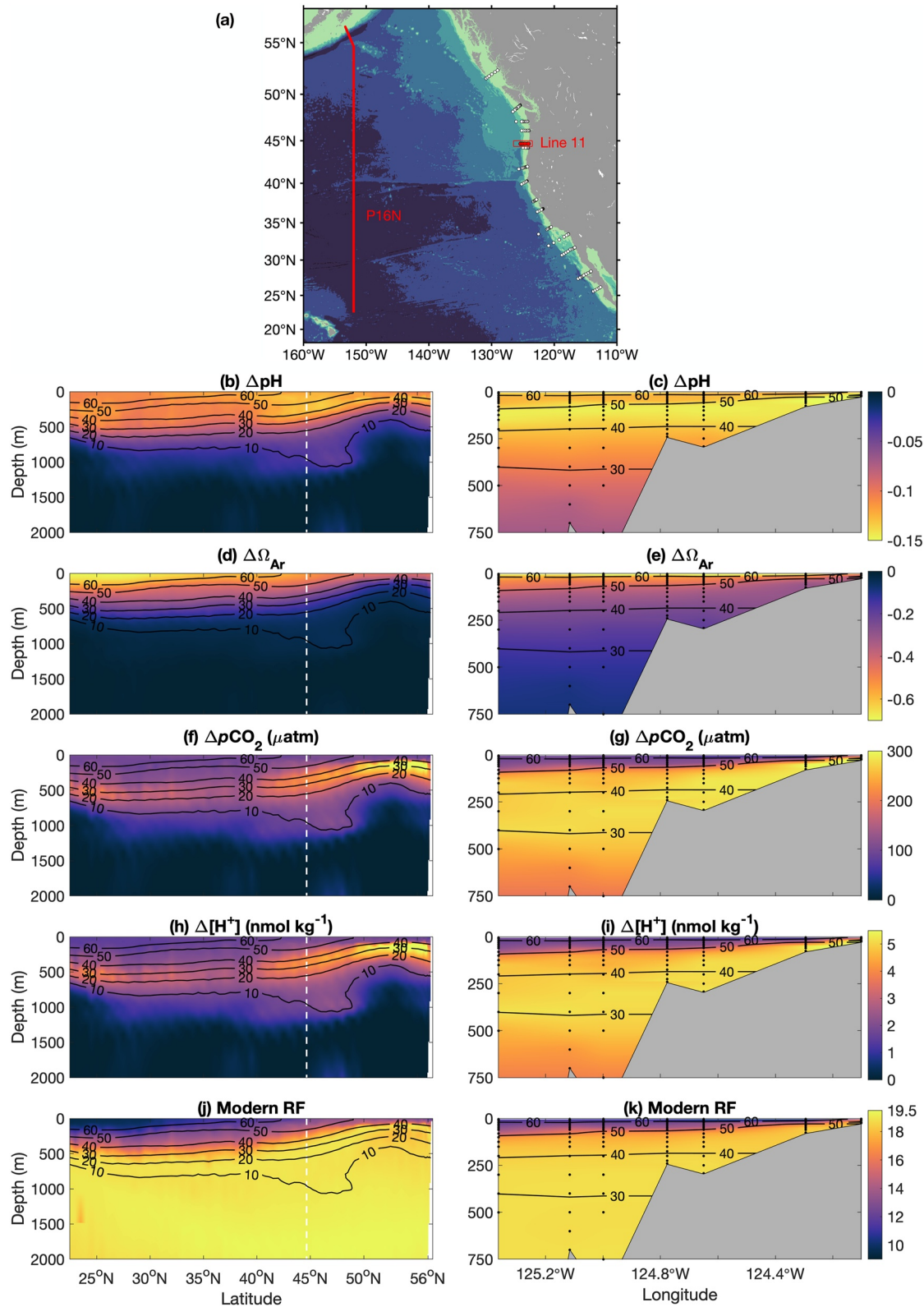
Figure 1. Changes (Δ) caused by C_{anth} (µmol kg^{-1}; contours) accumulation along (a; map) ~152°W in the Central North Pacific Ocean (left) and along Line 11 (~45°N) in the California Current Large Marine Ecosystem (right) for (b and c) pH, (d and e) Ω_{Ar}, (f and g) pCO$_2$, and (h and i) [H$^+$]. Panels (j and k) show modern Revelle Factors (RFs). Dashed white lines in the left panels mark the Central North Pacific Ocean data at 45°N shown in Figure 2.

2.2. Estimating C_{anth} in the CNPO and CCLME

C_{anth} distributions were estimated in the CCLME using a variant on the approach described by Carter et al. (2019). This method utilizes ensembles of extended Multiple Linear Regressions from 14 repeat hydrographic sections in the Pacific Ocean between 1991 and 2017 to estimate decadal C_{anth} accumulation along these various sections, including those in the CCLME. These estimates were then added to the 1994 C_{anth} estimates determined from the ΔC^* technique (Sabine et al., 2004), as regridded from the Global Ocean Data Analysis Project (GLODAP; Key et al., 2004), to yield modern C_{anth} values. Finally, the C_{anth} estimates are mapped temporally and spatially within the Pacific Ocean using regressions based on in situ temperature, salinity, and year. In contrast to the Carter et al. (2019) approach to map C_{anth} across the entire Pacific basin, depth was not used as a regression predictor for the US West Coast C_{anth} reconstructions due to seasonal coastal upwelling that links seawater properties more closely to density than to depth. This modification makes it more likely that surface C_{anth} estimates will be lower than expected from complete air-sea equilibrium, particularly in waters with salinities and temperatures characteristic of upwelling. We estimate an uncertainty of ~8 µmol kg^{-1} for C_{anth} in the CCLME (Text S1 in Supporting Information S1).

C_{anth} estimates for the CNPO during the 2015 P16 N cruise were obtained directly from the gridded product by Carter et al. (2017) and linearly interpolated onto the discrete sampling positions. Gridded C_{anth} values at 25 m were extrapolated to the surface. Unlike the approach used for the CCLME more broadly, this approach assumes surface C_{anth} keeps up with the expectations from complete equilibration with the atmospheric changes. Note that the C_{anth} estimated in the CCLME is offset from values estimated in the CNPO by 1 year due to different cruise years.

2.3. Determining the Impact of C_{anth} Accumulation

C_{anth} estimates were subtracted from modern, observed DIC concentrations to yield a PI DIC estimate. PI estimates of pH, Ω_{Ar}, pCO_2, and [H$^+$] were computed from PI DIC and modern TA using CO2SYS as described above. The impacts of C_{anth} accumulation on the carbonate system were evaluated by computing the change in pH, Ω_{Ar}, pCO_2, and [H$^+$] between the modern and PI values (e.g., $\Delta pH = pH_{modern} - pH_{PI}$). This method only accounts for the influence of C_{anth} and does not consider physically or biologically induced changes in ocean biogeochemistry or changes in heat and freshwater fluxes since industrialization.

2.4. Tracking Hypercapnic Events in the CCLME With a Regional Ocean Model

Observations in the CCLME provide a snapshot of the spatial extent of hypercapnia ($pCO_2 \geq 1,000$ µatm). To estimate the modern spatiotemporal variability of hypercapnic events in the CCLME, we use a near real-time, 4-dimensional variational data assimilative model of the CCLME implemented using the Region Ocean Modeling System (ROMS; Moore, Arango, Broquet, Edwards, et al., 2011; Moore, Arango, Broquet, Powell et al., 2011; Moore et al., 2013). The model domain extends from 30°N–48°N and 134°W–115.5°W (Figure 1b) and has a horizontal resolution of 1/10° with 42 terrain-following vertical layers (Figure S1a in Supporting Information S1; Veneziani et al., 2009). The model reproduced the observed density field along each CCLME Line with high fidelity ($r \geq 0.81$; Figure S2 in Supporting Information S1) and was used to explore conditions over 10 simulation years (2011–2020).

The subsurface upper boundary for hypercapnic water in the observations is aligned with an average density of 1027.5 ± 0.7 kg m^{-3} (Figure S3 in Supporting Information S1). The depth of this density surface was tracked daily over the 10 year model period to estimate the frequency, intensity, and duration of hypercapnic events at the 200 m isobath (roughly the continental shelf break; Figure S1; Text S2 in Supporting Information S1). If this density surface shoals onto the continental shelf during seasonal upwelling events, or if respiration processes increase pCO_2 in the local subsurface waters, nearshore communities could be at risk for hypercapnia. Event frequency is defined as the number of days in a year that the hypercapnic density surface is shallower than 200 m. Event duration is defined as the number of consecutive days that the hypercapnic density surface is shallower than 200 m. Event intensity is defined as the local volume of hypercapnic water above 200 m. Events within 0.5° of latitude of the model boundaries were neglected to account for biases attributed to boundary conditions (Text S2 in Supporting Information S1).

3. Results and Discussion

3.1. Anthropogenic Changes in CNPO and CCLME Carbonate Chemistry

Depth-resolved changes in carbonate system parameters caused by C_{anth} accumulation in the CNPO are shown in Figure 1 (left). The highest C_{anth} values of $\sim58 \pm 8$ µmol kg^{-1} are found at the surface where C_{anth} is absorbed, with peaks in the subtropics where waters are most efficient at absorbing C_{anth} (Sabine et al., 2004). In the high latitudes, absorbed C_{anth} gets transported to the ocean interior for storage, primarily in the midlatitude thermocline, with modern concentrations of ~50 µmol kg^{-1} (Carter et al., 2019; Gruber et al., 2019; Khatiwala et al., 2013).

C_{anth} accumulation in the ocean leads to the formation of carbonic acid, a weak acid that dissociates and is partially neutralized by reaction with $[CO_3^{2-}]$, producing $[H^+]$ and bicarbonate. The effects of these chemical processes manifest as reductions in pH and Ω_{Ar}, predominantly in the near-surface ocean where C_{anth} values are greatest. As a result, the patterns of ΔpH and $\Delta\Omega_{Ar}$ are similar to the distribution of C_{anth}, with near-surface (upper 30 m) values ranging from -0.125 to -0.095 and from -0.70 to -0.40, respectively, in the CNPO (Figures 1b and 1d). Similar upper ocean declines of pH and Ω_{Ar} due to C_{anth} accumulation were found in the coastal CCLME (Figure 1; right). Surface ocean C_{anth} estimates in the CCLME ranged from 45 to 75 µmol kg^{-1} in 2016, with the highest values observed south of 30°N (Figure S4 in Supporting Information S1). Lower surface C_{anth} values were found adjacent to the coast near Cape Mendocino (40°N) and Pt. St. George (42°N), as seen in 2013 by Feely et al. (2016). This heterogeneity in surface C_{anth} values, which is also found in the vertical C_{anth} gradient, can be explained by seasonal, nonuniform coastal upwelling in the CCLME that lifts subsurface water carrying lower C_{anth} to shallower depths along the coast. In the CCLME, near-surface (upper 30 m) values of ΔpH and $\Delta\Omega_{Ar}$ ranged between -0.160 to -0.116 and -0.72 to -0.34, respectively, along Line 11 (Figures 1c and 1e), which is within the ranges found for the entire CCLME domain (ΔpH: -0.167 to -0.095; $\Delta\Omega_{Ar}$: -0.74 to -0.29).

Unlike $\Delta\Omega_{Ar}$, the maximum change in pH is not always at the surface, but sometimes in the shallow subsurface in both the open (~200 m; Carter et al., 2019) and coastal (~100 m) oceans. This result agrees with findings of Lauvset et al. (2020) who performed a similar analysis for interior ΔpH and $\Delta\Omega_{Ar}$ using the GLODAPv2 gridded climatology with C_{anth} values for 2002 (Lauvset et al., 2016). A larger subsurface ΔpH reflects the enhanced sensitivity of pH to changes in C_{anth} (i.e., DIC) at depth, where the ratio of DIC to TA is higher than that at the surface (see Figure 7 of Lauvset et al., 2020). However, these larger changes in shallow, subsurface pH are of very similar magnitude to surface pH changes.

The vertical patterns of ΔpCO$_2$ and $\Delta[H^+]$ are distinct from those exhibited by ΔpH and $\Delta\Omega_{Ar}$ (Figures 1f–1i). The largest changes in pCO$_2$ and $[H^+]$ in the open ocean typically occur well below the surface (~100–600 m) coincident with lower C_{anth} (30–45 µmol kg^{-1}), a feature that extends to the subsurface CCLME (~240–400 m). The greatest ΔpCO$_2$ and $\Delta[H^+]$ along ~152°W exceed 275 µatm and 4.5 nmol kg^{-1}, respectively, in the CNPO (See Figure 4 of Fassbender et al., 2021) between a depth range of ~100 and ~200 m above 50°N. Lower maxima values of 175 µatm and 3.5 nmol kg^{-1} between ~400 and ~600 m are found in the northern mid-latitudes (20–40°N). In the CCLME along Line 11, increases in pCO$_2$ and $[H^+]$ ranged between 70–200 µatm and 1.3–3.5 nmol kg^{-1}, respectively, within the upper 80 m where $C_{anth} \geq 50$ µmol kg^{-1} (excluding the station closest to shore). On this transect, maximal values for ΔpCO$_2$ of ~250 µatm and for $\Delta[H^+]$ of 5.2 nmol kg^{-1} were found below this depth (~240 m; excluding the station closest to shore). These observed subsurface pCO$_2$ changes are larger than the atmospheric pCO$_2$ increase caused by human activites (from ~280 µatm to ~420 µatm $= \sim140$ µatm). In both the open and coastal oceans, the subsurface maximum in $\Delta[H^+]$ is not coincident with a subsurface maximum in ΔpH. This is because ΔpH reflects a relative, rather than absolute, change in $[H^+]$ and thus depends on the initial $[H^+]$ conditions (Fassbender et al., 2021).

The reason that pCO$_2$ and $[H^+]$ are more sensitive to smaller, subsurface C_{anth} changes in the open and coastal North Pacific is related to the background chemistry of these waters. The ocean's ability to buffer the chemical changes imposed by C_{anth} addition is often quantified using the Revelle sensitivity Factor (Broecker et al., 1979; Egleston et al., 2010; Fassbender et al., 2017; Middelburg et al., 2020; Revelle & Suess, 1957; Sabine et al., 2004). RF is defined as the ratio between a fractional change in pCO$_2$ and a fractional change in DIC for a given carbonate system perturbation, assuming constant alkalinity:

$$\text{RF} = \frac{\partial p\text{CO}_2/p\text{CO}_2}{\partial \text{DIC}/\text{DIC}} \tag{1}$$

A low RF value indicates a larger relative DIC change will occur for a given, relative pCO_2 perturbation, and signifies a greater capacity of the ocean to absorb anthropogenic CO_2 from the atmosphere. In contrast, waters with high RF values will be less efficient at absorbing anthropogenic atmospheric CO_2. Under the same construct, this also means that waters with different RF values that experience the same relative DIC perturbation will exhibit different relative pCO_2 changes (Fassbender et al., 2017, 2018).

Large gradients in RF have been identified across the global surface ocean (Bittig et al., 2018; Fassbender et al., 2017; Jiang et al., 2019; Sabine et al., 2004). Surface RFs in the CNPO are low in the warm tropics (∼10) and increase toward the cold poles (∼16), reflecting regional variability in carbon uptake efficiency (Figure 1j). RF values similarly increase with depth and toward the poles below the main thermocline, reaching a maximum of ∼19 below 1,000 m in the CNPO. These high subsurface RF values of 18 to 19 extend to the coastal CCLME (Figure 1k). High RF values are analogous to higher ratios of DIC to TA (Broecker et al., 1979; Egleston et al., 2010), as there is a relatively lower proportion of $[CO_3^{2-}]$ and higher proportion of aqueous CO_2 among the species in the DIC pool. However, waters with similar RF values may exhibit dissimilar pCO_2 responses to identical relative changes in DIC. This is because the magnitude of ΔpCO_2 for a given increase in C_{anth} also depends on the background pCO_2 level, which can vary significantly depending on the aqueous CO_2 fraction of DIC (Fassbender et al., 2017; Feely et al., 2018).

In the context of C_{anth} accumulation in the CNPO, the largest absolute changes in pCO_2 since industrialization are found between 200 and 600 m, despite lower C_{anth} values (20–30 μmol kg^{-1}) at these depths relative to the surface. Within this depth range, the CNPO has naturally elevated subsurface RF and pCO_2 values due to accumulated byproducts of organic matter remineralization, reflected by substantial O_2 utilization (Figure S5 in Supporting Information S1). Background RF and pCO_2 values remain high below this depth range; however, the magnitude of ΔpCO_2 decreases with depth in concert with declining C_{anth}. Like the open CNPO, CCLME subsurface waters are naturally elevated in RF and pCO_2 due to net respiration (Figure S6 in Supporting Information S1), and ΔpCO_2 values exhibit similar subsurface maxima. These findings suggest that opposing vertical gradients in the accumulation of C_{anth} and respiration byproducts create a particular depth range in which the pCO_2 sensitivity to DIC is elevated and the C_{anth} concentration is moderate, causing a subsurface ΔpCO_2 maximum in the open and coastal North Pacific. Since the $[H^+]$ and pCO_2 are tightly linked parameters, the patterns of $\Delta[H^+]$ are like those of ΔpCO_2 (Figure 2).

The patterns of chemical change in OA metrics are notably coherent in the CCLME, with similar magnitudes of subsurface ΔpCO_2 and $\Delta[H^+]$ increases throughout the domain (Figures 2e and 2f). Compared to the open CNPO at 45°N, maxima in ΔpCO_2 and $\Delta[H^+]$ in the CCLME appear shallower (∼280 vs. ∼400 m) and larger in magnitude (ΔpCO_2: 270 vs. 220 μatm; $\Delta[H^+]$: 4.9 vs. 3.8 nmol kg^{-1}; Figure 2). The average C_{anth} values at the depths of maximal ΔpCO_2 and $\Delta[H^+]$ in the open ocean and CCLME are similar (30–34 μmol kg^{-1}); however, the associated density surfaces carrying elevated background RF and pCO_2 are shallower nearshore due to the natural ocean physics (Figure S6 in Supporting Information S1). Though regional differences between the depth and magnitude of ΔpCO_2 and $\Delta[H^+]$ maxima are largely the result of circulation and upwelling, local processes in the CCLME may intensify the subsurface chemical response. Enhanced local organic matter remineralization caused by high levels of overlying primary production and a benthic boundary layer preventing export to depth can further increase subsurface pCO_2 on the continental shelf (Fassbender et al., 2011), leading to more pronounced responses to subsurface C_{anth} accumulation (Figure 3; Figure S7 in Supporting Information S1).

3.2. Expansion of the CCLME Hypercapnic Domain due to C_{anth} Accumulation

The changes in seawater chemistry due to C_{anth} accumulation have driven an increase in hypercapnic volume in the CNPO and CCLME. The minimum hypercapnic depth shoaled by 175 m (from 565 to 390 m) in the open ocean at 45°N, 152°W (Figure 2c) and by 185–300 m (from 435 to 200 m on average) in the CCLME (Figure 2g) compared to the PI mean minimum hypercapnic depths. This shoaling in the coastal region corresponds to a ∼73% average increase (range: 58%–94%) in the hypercapnic volume above 750 m between 25°N and 55°N, creating a modern coastal environment where 64%–100% of the hypercapnic water above 750 m is simultaneously hypoxic (Figure 2h). This expansion in the CCLME presently leaves, on average, ∼27% of the water column above 750 m as suitable habitat for marine organisms susceptible to hypercapnia.
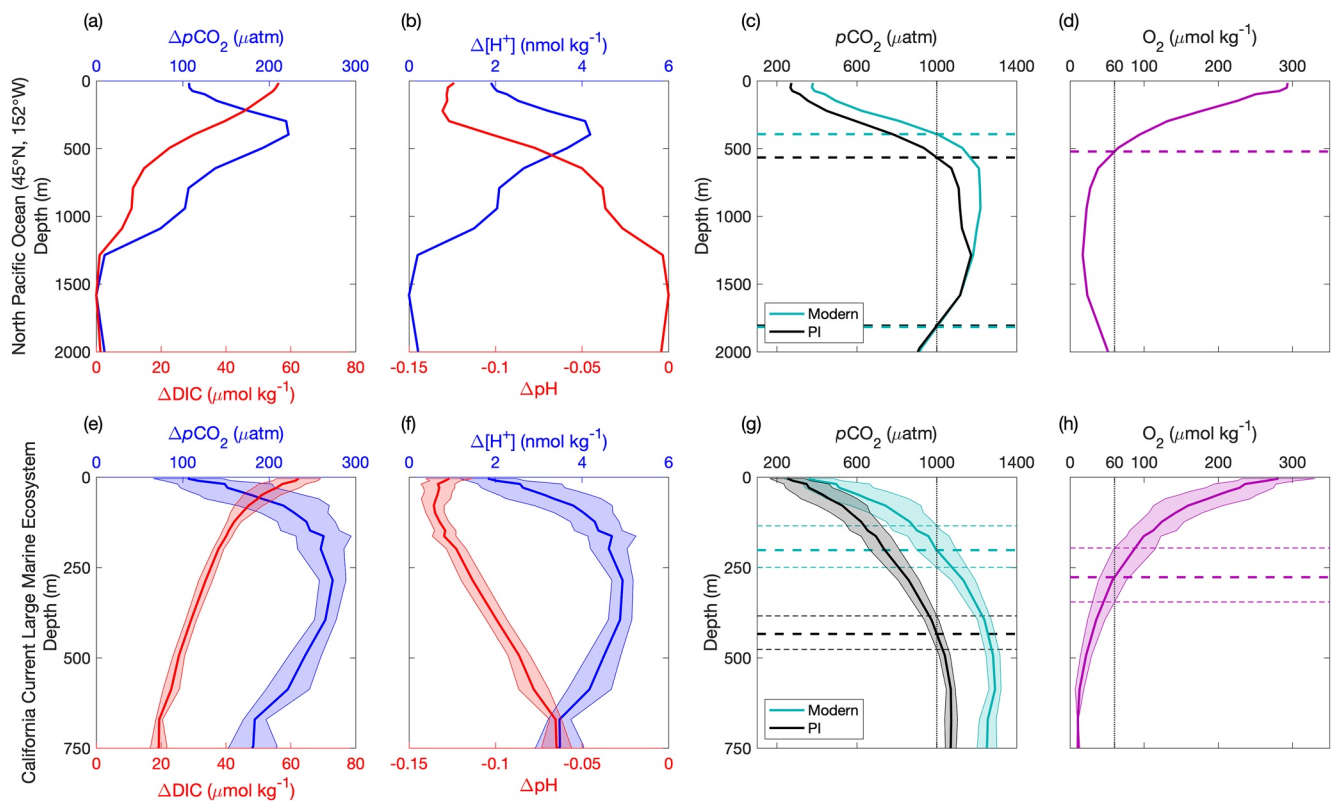
Figure 2. Profiles from the (top) upper 2000 m in the Central North Pacific Ocean at 45°N, 152°W and (bottom) upper 750 m in the California Current Large Marine Ecosystem (CCLME). The bold line in the lower panels indicates the average profile from all CCLME stations and shading represents ±1 standard deviation. The changes (Δ) due to C_{anth} accumulation are shown for (a and e) pCO_2 and dissolved inorganic carbon (DIC) and (b and f) $[H^+]$ and pH. (c and g). Modern (teal) and preindustrial (PI, black) pCO_2 and corresponding depth ranges (dashed lines) for hypercapnia ($pCO_2 \geq 1{,}000$ µatm, vertical line). (d and h) Modern (pink) O_2 and corresponding depth range (dashed lines) for hypoxia ($[O_2] \leq 60$ µmol kg^{-1}, vertical line).

By tracking the shallowest density layer on which hypercapnia was observed during WCOA2016 in model simulations, we find that hypercapnic events at the 200 m isobath have occurred throughout most of the domain between 2011 and 2020 (Figure 4). On average, events were most frequent in the northern region (north of Cape Mendocino), where hypercapnic conditions were present up to 180 days per year (Figure 4a) and certain individual events lasted for 3–4 months (Figure 4b). During intense events, up to 40% of the local water column (120–200 m) experienced hypercapnic conditions (Figure 4c). In contrast, events were less frequent and of shorter duration in the southern CCLME (south of Point Conception), occurring less than 20 days per year and lasting up to 3 days, on average. However, these short-lived events can still be intense, with up to 25% of the water column being hypercapnic (150–200 m). Less intense (<10% of the water column) and relatively short-lived (<5 days) events occurred, on average, in the central region (between Cape Mendocino and Point Conception), where hypercapnia was experienced for up to 40 days per year.

The timing of the most intense hypercapnic events in the CCLME may be influenced by seasonal variations of the hypercapnic density surface depth in response to the alongshore pressure gradient, modulated by wind stress forcing (Figure 4e; Figures S10 to S14 in Supporting Information S1). Between 2011 and 2020, the month of maximum hypercapnia intensity was tracked at each model grid along the 200 m isobath (n = 1,112; Figure 4e). During winter and early spring (December–March), the hypercapnic density surface may reside above the 200 m isobath in certain locations, preconditioning the local water column with hypercapnic water at depth (Figures S10 to S12 in Supporting Information S1). During these months in the central and southern domains, intermittent upwelling events induced by weak equatorward winds (or the relaxation of downwelling-favorable winds; Figures S13 and S14 in Supporting Information S1), generated the most intense hypercapnic events. In contrast, downwelling-favorable alongshore wind stress during the winter months in the northern domain may suppress hypercapnic events at the 200 m isobath. In this northern region, the most intense hypercapnic events occurred
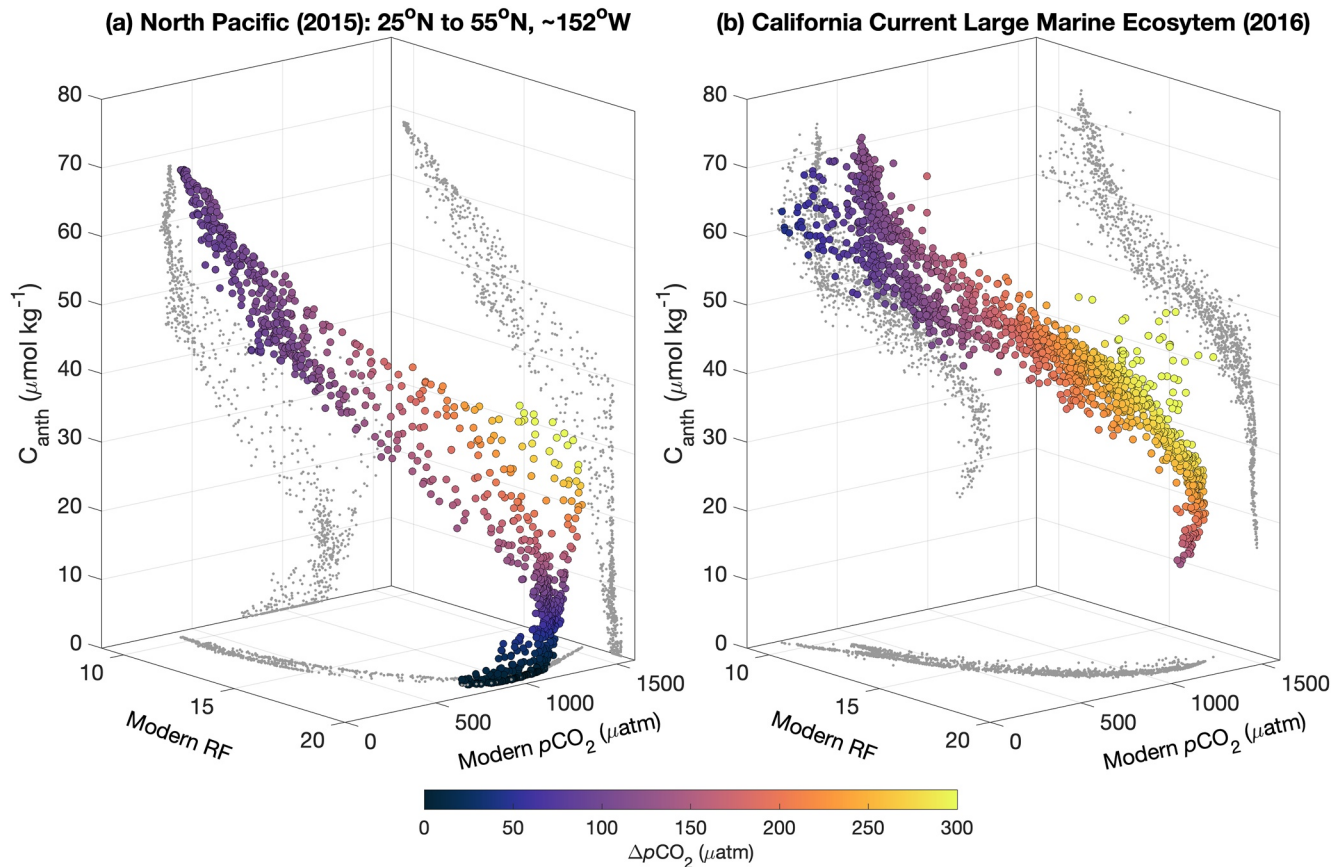
Figure 3. The change in pCO_2 (ΔpCO_2) due to C_{anth} accumulation in relationship to modern Revelle Factor (RF) and pCO_2 in the (a) Central North Pacific Ocean between 25°N and 55°N, ~152°W from P16 N and (b) the California Current Large Marine Ecosystem (CCLME) from WCOA2016.

in March–August, when winds shift predominantly equatorward along the coast and uplift subsurface isopycnals to shallower depths. The resulting alongshore pressure gradient in response to upwelling favorable conditions progressively deepened the isopycnal structure at the 200 m isobath from north to south in the central and southern domains, suppressing the occurrence of hypercapnic events at the 200 m isobath in spring and summer.

The metrics describing hypercapnic events in the CCLME only consider high pCO_2 waters delivered from offshore, physical sources by determining the shallowest density layer on which hypercapnia is observed. Though this density typically was not found inshore of the 200 m isobath in the model simulations, hypercapnia was observed inshore of the 200 m isobath during WCOA2016 (Figure S8 in Supporting Information S1). Assuming that the data-assimilative model simulations capture the physical dynamics of upwelling, this suggests that observed nearshore hypercapnia is further intensified by local organic matter respiration on the continental shelf that contributes to elevated subsurface pCO_2 (Fassbender et al., 2011; Feely et al., 2018; Figure S7 in Supporting Information S1).

4. Conclusion

While many studies focus on changes in pH and Ω_{Ar} to assess the progression of OA, our findings illustrate that these and other OA metrics (i.e., pCO_2 and [H+]) display different vertical sensitivities to C_{anth} accumulation within the water column. The CNPO and CCLME are particularly chemically sensitive to anthropogenic perturbations at depth, leading to the quantifiable intensification of subsurface pCO_2 and [H+] levels. The enhanced sensitivities are due to the age of the waters at mid-depths and the associated accumulation of byproducts from organic matter remineralization, which elevate subsurface pCO_2 and reduce the ocean buffering capacity. Subsurface pCO_2 intensification is relevant to the CCLME where pervasive hypercapnia may be introduced from offshore sources and subsequently enhanced by local remineralization processes. We find that the minimum
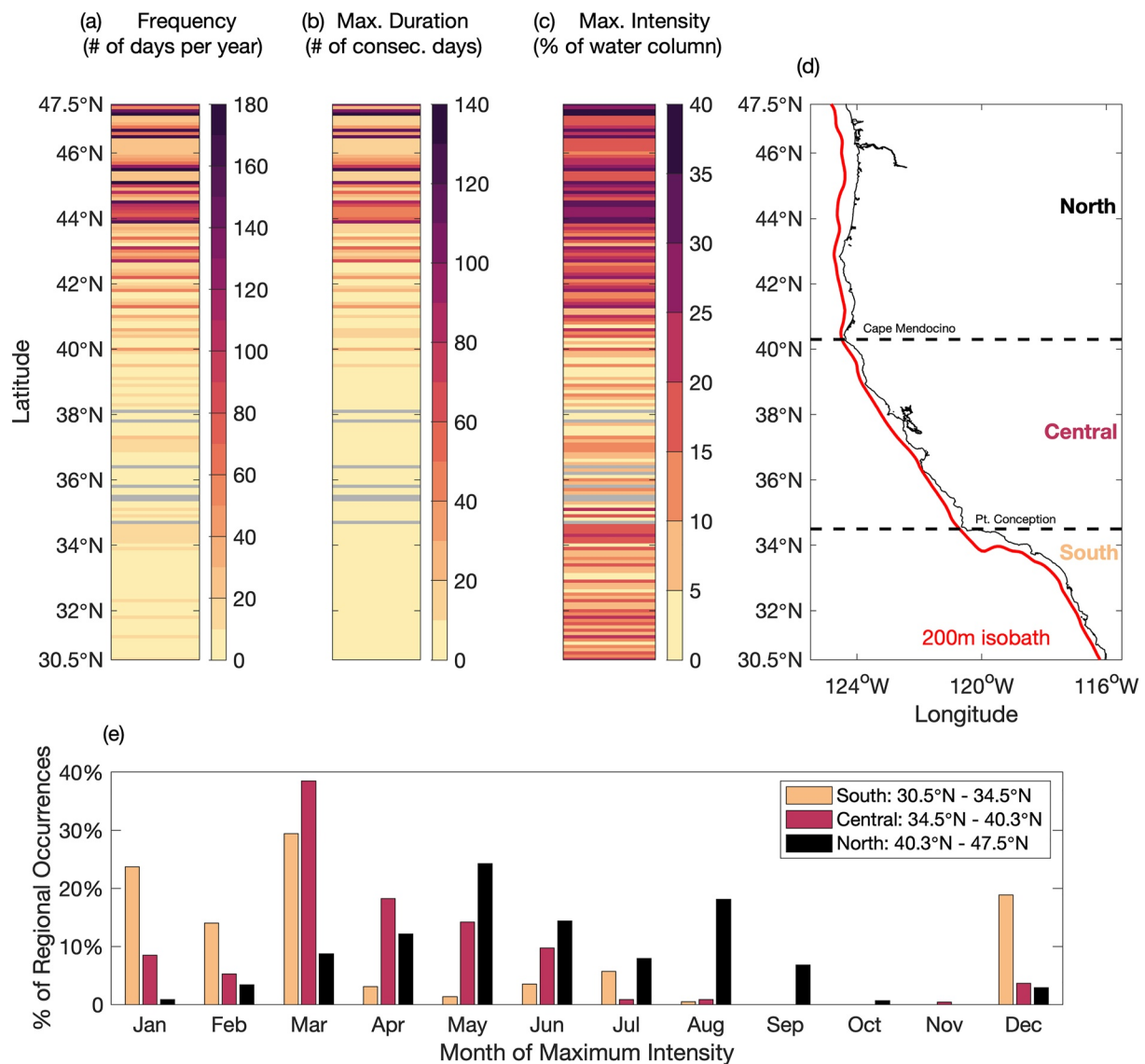
Figure 4. Hypercapnic events at the 200 m isobath in the California Current Large Marine Ecosystem (CCLME) estimated from daily output of a data-assimilative regional ocean circulation model. Annual event metrics of (a) frequency, (b) maximum duration, and (c) maximum intensity were averaged between 2011 and 2020. Gray indicates no hypercapnic event occurred at the 200 m isobath between 2011 and 2020. (d) Map of the 200 m isobath (red) and CCLME region delineation following that by Checkley and Barth (2009): southern (30.5°N–34.5°N); central (34.5°N–40.3°N); and northern (40.3°N–47.5°N). (e) Percentage of total regional hypercapnic events between 2011 and 2020 that the maximum hypercapnic intensity occurred in a given month on the 200 m isobath.

hypercapnic depth has shoaled by an average of 73% (to 200 m) in the upper 750 m of the CCLME since the PI era between 25°N and 50°N. Hypercapnia is predicted to increase in the CCLME (Feely et al., 2018) and globally (McNeil & Sasse, 2016) with continued C_{anth} accumulation, and thus will become an increasingly important stressor to susceptible pelagic and benthic communities. Consideration of multiple OA metrics, including pCO_2 and [H$^+$], supports a more complete characterization of the extent of subsurface anthropogenic chemical change.

Data Availability Statement

The observational data used in this study are publicly available through NOAA's National Centers for Environmental Information for CLIVAR/GO-SHIP P16 N Leg 2 cruise in 2015 (NCEI Accession: 0163182; https://doi.org/10.3334/cdiac/otg.go_ship_p16n_2015) and WCOA 2016 (NCEI Accession: 0208230; https://doi.org/10.7289/v5v40shg). Near real-time model output for the California Current Large Marine

Ecosystem are available through the UCSC Ocean Modelling and Data Assimilation Group (https://oceanmodeling.ucsc.edu:8443/thredds/dodsC/ccsra_2016a_phys_agg_slevs/fmrc/CCSRA_2016a_Phys_ROMS_Sigma-level_Aggregation_best.ncd.html). Anthropogenic carbon estimates from P16 N were accessed from Supporting Information S1 by Carter et al. (2017).

References

Alin, S. R., Feely, R. A., Hales, B., Byrne, R. H., Cochlan, W., Liu, X., & Greeley, D. (2017). Dissolved inorganic carbon, total alkalinity, pH on total scale, and other variables collected from profile and discrete sample observations using CTD, Niskin bottle, and other instruments from NOAA Ship Ronald H. Brown in the U.S. West Coast California Current System from 2016-05-08 to 2016-06-06 (NCEI Accession 0169412). NOAA National Centers for Environmental Information. [Dataset]. https://doi.org/10.7289/v5v40shg

Bates, N. R., Astor, Y. M., Church, M. J., Currie, K., Dore, J. E., González-Dávila, M., et al. (2014). A time-series view of changing surface ocean chemistry due to ocean uptake of anthropogenic CO_2 and ocean acidification. *Oceanography*, *27*(1), 126–141. https://doi.org/10.5670/oceanog.2014.16

Bittig, H. C., Steinhoff, T., Claustre, H., Fiedler, B., Williams, N. L., Sauzède, R., et al. (2018). An alternative to static climatologies: Robust estimation of open ocean CO_2 variables and nutrient concentrations from T, S, and O_2 data using Bayesian neural networks. *Frontiers in Marine Science*, *5*(SEP), 328. https://doi.org/10.3389/fmars.2018.00328

Broecker, W. S., Takahashi, T., Simpson, H. J., & Peng, T.-H. (1979). Fate of fossil fuel carbon dioxide and the global carbon budget. *Science*, *206*(4417), 409–418. https://doi.org/10.1126/science.206.4417.409

Cai, W. J., Hu, X., Huang, W. J., Murrell, M. C., Lehrter, J. C., Lohrenz, S. E., et al. (2011). Acidification of subsurface coastal waters enhanced by eutrophication. *Nature Geoscience*, *4*(11), 766–770. https://doi.org/10.1038/ngeo1297

Cai, W. J., Xu, Y. Y., Feely, R. A., Wanninkhof, R., Jönsson, B., Alin, S. R., et al. (2020). Controls on surface water carbonate chemistry along North American ocean margins. *Nature Communications*, *11*(1), 2691. https://doi.org/10.1038/s41467-020-16530-z

Caldeira, K., & Wickett, M. E. (2003). Anthropogenic carbon and ocean pH. *Nature*, *425*(6956), 365. https://doi.org/10.1038/425365a

Carpenter, J. H. (1965). The Chesapeake Bay Institute technique for the winkler dissolved oxygen method. *Limnology & Oceanography*, *10*(1), 141–143. https://doi.org/10.4319/lo.1965.10.1.0141

Carter, B. R., Feely, R. A., Mecking, S., Cross, J. N., Macdonald, A. M., Siedlecki, S. A., et al. (2017). Two decades of Pacific anthropogenic carbon storage and Ocean acidification along Global Ocean Ship-based hydrographic investigations program sections P16 and P02. *Global Biogeochemical Cycles*, *31*(2), 306–327. https://doi.org/10.1002/2016GB005485

Carter, B. R., Feely, R. A., Wanninkhof, R., Kouketsu, S., Sonnerup, R. E., Pardo, P. C., et al. (2019). Pacific anthropogenic carbon between 1991 and 2017. *Global Biogeochemical Cycles*, *33*(5), 597–617. https://doi.org/10.1029/2018GB006154

Chan, F., Barth, J. A., Blanchette, C. A., Byrne, R. H., Chavez, F., Cheriton, O., et al. (2017). Persistent spatial structuring of coastal ocean acidification in the California current system. *Scientific Reports*, *7*(1), 2526. https://doi.org/10.1038/s41598-017-02777-y

Chan, F., Barth, J. A., Kroeker, K. J., Lubchenco, J., & Menge, B. A. (2019). The dynamics and impact of ocean acidification and hypoxia: Insights from sustained investigations in the northern California current large marine ecosystem. *Oceanography*, *32*(3), 62–71. https://doi.org/10.5670/oceanog.2019.312

Checkley, D. M., & Barth, J. A. (2009). Patterns and processes in the California Current System. *Progress in Oceanography*, *83*(1–4), 49–64. https://doi.org/10.1016/j.pocean.2009.07.028

Cheresh, J., & Fiechter, J. (2020). Physical and Biogeochemical drivers of alongshore pH and oxygen variability in the California current system. *Geophysical Research Letters*, *47*(19), e2020GL089553. https://doi.org/10.1029/2020GL089553

Connolly, T. P., Hickey, B. M., Geier, S. L., & Cochlan, W. P. (2010). Processes influencing seasonal hypoxia in the northern California current system. *Journal of Geophysical Research*, *115*, 3021. https://doi.org/10.1029/2009JC005283

Cross, J. N., Macdonald, A. M., Alin, S. R., Wanninkhof, R., Dickson, A. G., Carlson, C. A., et al. (2017). Dissolved inorganic carbon (DIC), total alkalinity, pH on total scale, dissolved organic carbon (DOC), chlorofluorocarbons (CFC-11, CFC-12), temperature, salinity and other hydrographic and chemical variables collected from discrete samples and profile observations during NOAA Ship Ronald H. Brown cruise along the GO-SHIP Section P16N_2015, Legs 1 and 2 (EXPOCODEs 33RO20150410 and 33RO20150525) in the Pacific Ocean, from 2015-04-10 to 2015-06-27 (NCEI Accession 0163182). NOAA National Centers for Environmental Information[Dataset], https://doi.org/10.3334/cdiac/otg.go_ship_p16n_2015

Dickson, A. G. (1990). Standard potential of the reaction: AgCl(s) + 12H$_2$(g) = Ag(s) + HCl(aq), and and the standard acidity constant of the ion HSO_4^- in synthetic sea water from 273.15 to 318.15 K. *The Journal of Chemical Thermodynamics*, *22*(2), 113–127. https://doi.org/10.1016/0021-9614(90)90074-Z

Dickson, A. G., Afghan, J. D., & Anderson, G. C. (2003). Reference materials for oceanic CO_2 analysis: A method for the certification of total alkalinity. *Marine Chemistry*, *80*(2–3), 185–197. https://doi.org/10.1016/S0304-4203(02)00133-0

Dickson, A. G., Sabine, C. L., & Christian, J. R. (2007). *Guide to best practices for ocean CO_2 measurements*. PICES Special Publication.

Doney, S. C., Busch, D. S., Cooley, S. R., & Kroeker, K. J. (2020). The impacts of ocean acidification on marine ecosystems and reliant human communities. *Annual Review of Environment and Resources*, *45*(1), 83–112. https://doi.org/10.1146/annurev-environ-012320-083019

Egleston, E. S., Sabine, C. L., & Morel, F. M. M. (2010). Revelle revisited: Buffer factors that quantify the response of ocean chemistry to changes in DIC and alkalinity. *Global Biogeochemical Cycles*, *24*(1). https://doi.org/10.1029/2008GB003407

Fassbender, A. J., Orr, J. C., & Dickson, A. G. (2021). Technical note: Interpreting pH changes. *Biogeosciences*, *18*(4), 1407–1415. https://doi.org/10.5194/bg-18-1407-2021

Fassbender, A. J., Rodgers, K. B., Palevsky, H. I., & Sabine, C. L. (2018). Seasonal asymmetry in the evolution of surface ocean pCO$_2$ and pH Thermodynamic drivers and the influence on sea-air CO_2 Flux. *Global Biogeochemical Cycles*, *32*(10), 1476–1497. https://doi.org/10.1029/2017GB005855

Fassbender, A. J., Sabine, C. L., Feely, R. A., Langdon, C., & Mordy, C. W. (2011). Inorganic carbon dynamics during northern California coastal upwelling. *Continental Shelf Research*, *31*(11), 1180–1192. https://doi.org/10.1016/j.csr.2011.04.006

Fassbender, A. J., Sabine, C. L., & Palevsky, H. I. (2017). Nonuniform ocean acidification and attenuation of the ocean carbon sink. *Geophysical Research Letters*, *44*(16), 8404–8413. https://doi.org/10.1002/2017GL074389

Feely, R. A., Alin, S. R., Carter, B., Bednaršek, N., Hales, B., Chan, F., et al. (2016). Chemical and biological impacts of ocean acidification along the west coast of North America. *Estuarine, Coastal and Shelf Science*, *183*, 260–270. https://doi.org/10.1016/j.ecss.2016.08.043

Feely, R. A., Doney, S. C., & Cooley, S. R. (2009). Ocean acidification: Present conditions and future changes in a high-CO_2 world. *Oceanography*, *22*(4), 36–47. https://doi.org/10.5670/oceanog.2009.95

Feely, R. A., Okazaki, R. R., Cai, W. J., Bednaršek, N., Alin, S. R., Byrne, R. H., & Fassbender, A. (2018). The combined effects of acidification and hypoxia on pH and aragonite saturation in the coastal waters of the California current ecosystem and the northern Gulf of Mexico. *Continental Shelf Research*, *152*, 50–60. https://doi.org/10.1016/j.csr.2017.11.002

Feely, R. A., Sabine, C. L., Hernandez-Ayon, J. M., Ianson, D., & Hales, B. (2008). Evidence for upwelling of corrosive "acidified" water onto the continental shelf. *Science*, *320*(5882), 1490–1492. https://doi.org/10.1126/science.1155676

Feely, R. A., Sabine, C. L., Lee, K., Berelson, W., Kleypas, J., Fabry, V. J., & Millero, F. J. (2004). Impact of anthropogenic CO_2 on the $CaCO_3$ system in the oceans. *Science*, *305*(5682), 362–366. https://doi.org/10.1126/science.1097329

Friedlingstein, P., Jones, M. W., O'Sullivan, M., Andrew, R. M., Bakker, D. C. E., Hauck, J., et al. (2022). Global carbon budget 2021. *Earth System Science Data*, *14*(4), 1917–2005. https://doi.org/10.5194/ESSD-14-1917-2022

Gattuso, J.-P., Magnan, A., Billé, R., Cheung, W. W. L., Howes, E. L., Joos, F., et al. (2015). Contrasting futures for ocean and society from different anthropogenic CO_2 emissions scenarios. *Science*, *349*(6243). https://doi.org/10.1126/science.aac4722

Grantham, B. A., Chan, F., Nielsen, K. J., Fox, D. S., Barth, J. A., Huyer, A., et al. (2004). Upwelling-driven nearshore hypoxia signals ecosystem and oceanographic changes in the northeast Pacific. *Nature*, *429*(6993), 749–754. https://doi.org/10.1038/nature02605

Gruber, N., Clement, D., Carter, B. R., Feely, R. A., van Heuven, S., Hoppema, M., et al. (2019). The oceanic sink for anthropogenic CO_2 from 1994 to 2007. *Science*, *363*(6432), 1193–1199. https://doi.org/10.1126/science.aau5153

Gruber, N., Hauri, C., Lachkar, Z., Loher, D., Frölicher, T. L., & Plattner, G. K. (2012). Rapid progression of ocean acidification in the California current system. *Science*, *337*(6091), 220–223. https://doi.org/10.1126/science.1216773

Hagens, M., & Middelburg, J. J. (2016). Generalised expressions for the response of pH to changes in ocean chemistry. *Geochimica et Cosmochimica Acta*, *187*, 334–349. https://doi.org/10.1016/J.GCA.2016.04.012

Hauri, C., Gruber, N., Plattner, G. K., Alin, S., Feely, R. A., Hales, B., & Wheeler, P. A. (2009). Ocean acidification in the California current system. *Oceanography*, *22*(4), 60–71. https://doi.org/10.5670/oceanog.2009.97

Hauri, C., Gruber, N., Vogt, M., Doney, S. C., Feely, R. A., Lachkar, Z., et al. (2013). Spatiotemporal variability and long-term trends of ocean acidification in the California current system. *Biogeosciences*, *10*(1), 193–216. https://doi.org/10.5194/bg-10-193-2013

Jiang, L. Q., Carter, B. R., Feely, R. A., Lauvset, S. K., & Olsen, A. (2019). Surface ocean pH and buffer capacity: Past, present and future. *Scientific Reports*, *9*(1), 1–11. https://doi.org/10.1038/s41598-019-55039-4

Jiang, L. Q., Feely, R. A., Carter, B. R., Greeley, D. J., Gledhill, D. K., & Arzayus, K. M. (2015). Climatological distribution of aragonite saturation state in the global oceans. *Global Biogeochemical Cycles*, *29*(10), 1656–1673. https://doi.org/10.1002/2015GB005198

Johnson, K. M., Wills, K. D., Butler, D. B., Johnson, W. K., & Wong, C. S. (1993). Coulometric total carbon dioxide analysis for marine studies: Maximizing the performance of an automated gas extraction system and coulometric detector. *Marine Chemistry*, *44*(2–4), 167–187. https://doi.org/10.1016/0304-4203(93)90201-X

Key, R. M., Kozyr, A., Sabine, C. L., Lee, K., Wanninkhof, R., Bullister, J. L., et al. (2004). A global ocean carbon climatology: Results from global data analysis project (GLODAP). *Global Biogeochemical Cycles*, *18*(4), 1–23. https://doi.org/10.1029/2004GB002247

Khatiwala, S., Tanhua, T., Mikaloff Fletcher, S., Gerber, M., Doney, S. C., Graven, H. D., et al. (2013). Global ocean storage of anthropogenic carbon. *Biogeosciences*, *10*(4), 2169–2191. https://doi.org/10.5194/bg-10-2169-2013

Kroeker, K. J., Kordas, R. L., Crim, R., Hendriks, I. E., Ramajo, L., Singh, G. S., et al. (2013). Impacts of ocean acidification on marine organisms: Quantifying sensitivities and interaction with warming. *Global Change Biology*, *19*(6), 1884–1896. https://doi.org/10.1111/gcb.12179

Lauvset, S. K., Carter, B. R., Perez, F. F., Jiang, L. Q., Feely, R. A., Velo, A., & Olsen, A. (2020). Processes driving global interior ocean pH Distribution. *Global Biogeochemical Cycles*, *34*(1), e2019GB006229. https://doi.org/10.1029/2019GB006229

Lauvset, S. K., Gruber, N., Landschützer, P., Olsen, A., & Tjiputra, J. (2015). Trends and drivers in global surface ocean pH over the past 3 decades. *Biogeosciences*, *12*(5), 1285–1298. https://doi.org/10.5194/bg-12-1285-2015

Lauvset, S. K., Key, R. M., Olsen, A., Van Heuven, S., Velo, A., Lin, X., et al. (2016). A new global interior ocean mapped climatology: The 1°×1° GLODAP version 2. *Earth System Science Data*, *8*(2), 325–340. https://doi.org/10.5194/essd-8-325-2016

Lewis, E., & Wallace, D. W. R. (1998). *CO2SYS - program developed for the CO_2 system calculations*. ORNL/CDIAC-105 (Ed Center CDIA).

Lueker, T. J., Dickson, A. G., & Keeling, C. D. (2000). Ocean pCO_2 calculated from dissolved inorganic carbon, alkalinity, and equations for K_1 and K_2: Validation based on laboratory measurements of CO_2 in gas and seawater at equilibrium. *Marine Chemistry*, *70*(1–3), 105–119. https://doi.org/10.1016/S0304-4203(00)00022-0

McNeil, B. I., & Sasse, T. P. (2016). Future ocean hypercapnia driven by anthropogenic amplification of the natural CO_2 cycle. *Nature*, *529*(7586), 383–386. https://doi.org/10.1038/nature16156

Middelburg, J. J., Soetaert, K., & Hagens, M. (2020). Ocean Alkalinity, buffering and biogeochemical processes. *Reviews of Geophysics*, *58*(3), e2019RG000681. https://doi.org/10.1029/2019RG000681

Millero, F. J., Zhang, J. Z., Lee, K., & Campbell, D. M. (1993). Titration alkalinity of seawater. *Marine Chemistry*, *44*(2–4), 153–165. https://doi.org/10.1016/0304-4203(93)90200-8

Moore, A. M., Arango, H. G., Broquet, G., Edwards, C., Veneziani, M., Powell, B., et al. (2011). The regional ocean modeling system (ROMS) 4-dimensional variational data assimilation systems. Part II - performance and application to the California Current System. *Progress in Oceanography*, *91*(1), 50–73. https://doi.org/10.1016/j.pocean.2011.05.003

Moore, A. M., Arango, H. G., Broquet, G., Powell, B. S., Weaver, A. T., & Zavala-Garay, J. (2011). The regional ocean modeling system (ROMS) 4-dimensional variational data assimilation systems: Part I – System overview and formulation. *Progress in Oceanography*, *91*(1), 34–49. https://doi.org/10.1016/J.POCEAN.2011.05.004

Moore, A. M., Edwards, C. A., Fiechter, J., Drake, P., Neveu, E., Arango, H. G., et al. (2013). A 4D-var analysis system for the California current: A prototype for an operational regional ocean data assimilation system. *Data Assimilation for Atmospheric, Oceanic and Hydrologic Applications*, *II*, 345–366. https://doi.org/10.1007/978-3-642-35088-7_14

Nilsson, G. E., Dixson, D. L., Domenici, P., McCormick, M. I., Sørensen, C., Watson, S. A., & Munday, P. L. (2012). Near-future carbon dioxide levels alter fish behavior by interfering with neurotransmitter function. *Nature Climate Change*, *2*(3), 201–204. Nature Publishing Group. https://doi.org/10.1038/nclimate1352

Orr, J. C., Fabry, V. J., Aumont, O., Bopp, L., Doney, S. C., Feely, R. A., et al. (2005). Anthropogenic ocean acidification over the twenty-first century and its impact on calcifying organisms. *Nature*, *437*(7059), 681–686. https://doi.org/10.1038/nature04095

Perry, S. F., & Gilmour, K. M. (2006). Acid-base balance and CO_2 excretion in fish: Unanswered questions and emerging models. *Respiratory Physiology & Neurobiology*, *154*(1–2), 199–215. https://doi.org/10.1016/j.resp.2006.04.010

Peterson, J. O., Morgan, C. A., Peterson, W. T., & Di Lorenzo, E. (2013). Seasonal and interannual variation in the extent of hypoxia in the northern California Current from 1998-2012. *Limnology & Oceanography*, *58*(6), 2279–2292. https://doi.org/10.4319/lo.2013.58.6.2279

Resplandy, L., Bopp, L., Orr, J. C., & Dunne, J. P. (2013). Role of mode and intermediate waters in future ocean acidification: Analysis of CMIP5 models. *Geophysical Research Letters*, *40*(12), 3091–3095. https://doi.org/10.1002/grl.50414

Revelle, R., & Suess, H. E. (1957). Carbon dioxide exchange between atmosphere and ocean and the question of an increase of atmospheric CO_2 during the past decades. *Tellus*, *9*(1), 18–27. https://doi.org/10.1111/j.2153-3490.1957.tb01849.x

Riebesell, U., Rtzinger, A. K., & Oschlies, A. (2009). Sensitivities of marine carbon fluxes to ocean change. *Proceedings of the National Academy of Sciences of the United States of America*, *106*(49), 20602–20609. https://doi.org/10.1073/pnas.0813291106

Ríos, A. F., Resplandy, L., García-Ibáñez, M. I., Fajar, N. M., Velo, A., Padin, X. A., et al. (2015). Decadal acidification in the water masses of the Atlantic Ocean. *Proceedings of the National Academy of Sciences of the United States of America*, *112*(32), 9950–9955. https://doi.org/10.1073/pnas.1504613112

Sabine, C. L., Feely, R. A., Gruber, N., Key, R. M., Lee, K., Bullister, J. L., et al. (2004). The oceanic sink for anthropogenic CO_2. *Science*, *305*(5682), 367–371. https://doi.org/10.1126/science.1097403

Uppström, L. R. (1974). The boron/chlorinity ratio of deep-sea water from the Pacific Ocean. *Deep-Sea Research and Oceanographic Abstracts*, *21*(2), 161–162. https://doi.org/10.1016/0011-7471(74)90074-6

van Heuven, S., Pierrot, D., Rae, J. W. B., Lewis, E., & Wallace, D. W. R. (2011). *MATLAB program developed for CO_2 system calculations*. ORNL/CDIAC-105b. Carbon Dioxide Information Analysis Center, Oak Ridge National Laboratory, U.S. Department of Energy. https://doi.org/10.3334/CDIAC/otg.CO2SYS_MATLAB_v1.1

Veneziani, M., Edwards, C. A., Doyle, J. D., & Foley, D. (2009). A central California coastal ocean modeling study: 1. Forward model and the influence of realistic versus climatological forcing. *Journal of Geophysical Research*, *114*, 4015. https://doi.org/10.1029/2008JC004774

References From the Supporting Information

Carter, B. R., Feely, R. A., Lauvset, S. K., Olsen, A., DeVries, T., & Sonnerup, R. (2020). Preformed properties for marine organic matter and carbonate mineral cycling quantification. *Global Biogeochemical Cycles*, *35*(1), e2020GB006623. https://doi.org/10.1029/2020gb006623

Esbaugh, A. J., Heuer, R., & Grosell, M. (2012). Impacts of ocean acidification on respiratory gas exchange and acid–base balance in a marine teleost, Opsanus beta. *Journal of Comparative Physiology B*, *182*(7), 921–934. https://doi.org/10.1007/s00360-012-0668-5

Heuer, R. M., & Grosell, M. (2014). Physiological impacts of elevated carbon dioxide and ocean acidification on fish. *American Journal of Physiology - Regulatory, Integrative and Comparative Physiology*, *307*(9), R1061–R1084. https://doi.org/10.1152/ajpregu.00064.2014

Erratum

In the originally published version of this article, an incorrect reference, Dickson et al. (1990), was included in the reference list and cited in section 2.1, the second paragraph. The correct reference is Dickson (1990), which was not included in the reference list of the originally published version of the article. The correct reference and citation in text have since been substituted for the incorrect ones, and the present version may be considered the authoritative version of record.